Dewetting hydrodynamics in 1+1 dimensions

H. Müller-Krumbhaar, H. Emmerich,* E. Brener, and M. Hartmann
Institut für Festkörperforschung, Forschungszentrum Jülich, D-52425 Jülich, Germany
(Received 12 May 2000; revised manuscript received 13 October 2000; published 25 January 2001)

A model for the phase transition between partial wetting and dewetting of a substrate has been formulated that explicitly incorporates the hydrodynamic flow during the dewetting process in $1+1$ dimensions. The model simulates a fluid layer of finite thickness on a substrate in coexistence with a dry part of the substrate and a gas phase above the substrate. Under nonequilibrium ''dewetting'' conditions, the front between the dry part and the wet part of the surface moves towards the wet part inducing hydrodynamic flow inside the wet layer. In more general terms, the model handles two immiscible fluids with a freely movable interface in an inhomogeneous external force field. Handling the interface by a new variant of the phase-field model, we obtain an efficient code with well-defined interfacial properties. In particular, the (free) energy can be chosen at will. We demonstrate that our model works well in the viscosity range of creeping flow and we give qualitative results for the higher Reynolds numbers. Connections to experimental realizations are discussed.

DOI: 10.1103/PhysRevE.63.026304 PACS number(s): 47.20.Ma, 68.08.Bc, 64.60.My, 83.50.Lh

I. INTRODUCTION

Wetting and dewetting of a substrate by a film of fluid is a particularly interesting process of pattern formation with obvious significance in many technical applications of surface coating. In this phenomenon, various ingredients of equilibrium thermodynamics, diffusion and convection transport on different time scales, together with nonlocal effects and external fields have to be considered simultaneously. Furthermore, the freely mobile interface between the fluid wetting layer and the gas phase above the substrate is susceptible to various forces, leading to interface-driven instabilities such as, for example, the Marangoni effect.

In the phenomenon of *partial wetting* [1] considered here, a thin film of well-defined thickness is formed on the surface of a substrate. The forces responsible for this film are in addition to the cohesive forces between water molecule Van der Waals forces and polar forces [1–3] from the substrate. The statics and dynamics of such a film on a substrate have been discussed in detail, e.g., by Sharma and Jameel [4], Israelachvili [5], Forgacs *et al.* [1], and by De Gennes [2]. Recently, beautiful experiments have been performed by Lipson *et al.* [6], Herminghaus *et al.* [8], continuing and extending earlier work by Reiter [9] and Brochard-Wyart *et al.* [3]. In the experiments of Lipson's group [6], it was found that the patterns observed correspond to seaweed patterns discovered recently for the case of diffusional transport [10]. This is to be expected since in the limit of creeping flow corresponding to low Reynolds numbers or high viscosity, the hydrodynamic flow equation for dewetting degenerates to a diffusion equation with an effective diffusion constant inversely proportional to the viscosity. This is quite analogous to Darcy's law of flow in porous media.

As we have demonstrated, this effective diffusion equation, being of Cahn-Hilliard-type [11], corresponds in a linear approximation to the growth model studied in the context of two-dimensional interfacial pattern formation under isotropic conditions [10,12]. Our interest is now to understand what happens if the conditions for replacing the Navier-Stokes equations by an effective diffusion equation are no longer valid. For higher Reynolds numbers, significant changes due to increasing vorticity in the inertial range of wavelengths should be expected.

We have constructed a model together with a numerical scheme that allows us to treat the full Navier-Stokes equations for this wetting-dewetting problem. As a first step and to keep the computational effort as low as possible, the present investigation is still restricted to a $(1+1)$-dimensional system that corresponds to a planar cut perpendicular to the substrate. Therefore, it cannot be directly related to the pattern-formation experiments described above since these involve real three-dimensional instabilities and material redistribution. However, since our approach to the full dewetting problem even now incorporates the regime where the full Navier-Stokes equations come into play and dominate the overall behavior, it already can give first insights into the general physics of these systems, which have not been treated so far. Even though we are still restricted to a simple $(1+1)$-dimensional description, one still can think of experimental realizations where this geometry is enforced by some external conditions. A possible realization would be the dewetting of a thin film starting from a linear front, which is induced by a short heat pulse of a straight wire within the plane of the fluid. Clearly this description is only valid as long as no front instabilities occur. We plan to extend our model to a full three-dimensional description in order to facilitate pattern-formation simulations and quantitative comparisons to the experiments mentioned above.

Our x coordinate represents the direction parallel to the surface of the substrate, which is located at $z=0$. The z coordinate represents the normal direction away from the substrate into the gas phase. Since the energetic properties of the system are different close to the substrate and far away from the substrate, we have essentially to distinguish between three different phases: the remote gas phase, the wet layer on the substrate, and the dry region on the substrate.

*Present address: Max Planck Institut für komplexer Systeme, Dresden, Germany.

 ©2001 The American Physical Society

The latter two phases can be conveniently described by a tanh(x)-shaped height profile above the substrate as an envelope over the liquid film. In this sense the wet surface ($x \to \infty$) corresponds to a moderately thick fluid layer, while the dry surface ($x \to -\infty$) corresponds to an extremely thin fluid layer adsorbed on the substrate. The tanh-shaped profile then represents a front separating the wet and the dry region near $x=0$ under equilibrium conditions. (Of course, the precise profile finally results from the solution of the model; it may practically differ from a tanh form.) Under nonequilibrium conditions the profile will advance, hereby increasing the dry area on the substrate under dewetting conditions and vice versa.

The paper is organized as follows. In Sec. II, we describe the basic model in more detail. In Sec. III, we explain our general scheme of hydrodynamic modeling, which is followed by a section containing the specific modifications to handle the dewetting process (Sec. IV). In Sec. V, we present and discuss our first results.

II. BASIC MODEL IN CREEP FLOW

In this section, the effective equations of motion for a drying thin film originally wetting a substrate are summarized for the limit of high viscosity or creeping flow. These equations are equivalent to the one-sided model of diffusional growth with an effective diffusion coefficient that depends on the viscosity and on the thermodynamical properties of the thin film.

According to the description given in Sharma [4] and De Gennes [2], there is a possibility for the almost dry part of the solid substrate to be in equilibrium with the wet part, which is in fact a thin (but macroscopic) film of liquid. Both parts (dry and wet) on the solid substrate are separated by a front, which can be described by an interface height variable $h(x)$ with x being the coordinate across the front from the dry to the wet part. Towards the dry part, the height variable goes to a very small value h_-; towards the wet part, the film thickness goes to an equilibrium value $h_\infty(p)$ for given pressure p with a coexisting vapor phase. At a specific pressure p_0, the liquid film can additionally be in equilibrium with the (almost) dry surface. The corresponding thickness of the wet film is then defined as $h_0=h_\infty(p_0)$. For lower vapor pressure, the equilibrium film thickness $h_\infty(p)$ would decrease to a metastable value smaller than h_0. Therefore, the stable dry area would expand at the cost of the wet area. This is the dewetting phenomenon under consideration.

We assume a surface tension γ to exist between the liquid and the vapor. The free energy of the film can then be written as

$$G=\int \left\{ g(h(x,y))+\frac{\gamma}{2}|\nabla h|^2 \right\} dx\, dy, \tag{1}$$

where $g(h)$ has two minima, and x and y are coordinates within the plane of the substrate.

In equilibrium a double-tangent construction to $g(h)$ gives the two solutions h_- for the dry part and $h_0(p)$ for the wet part of the surface. This leads to the evolution equation [4,6] for the film variable $h(x,y;t)$:

$$\frac{\partial h}{\partial t}=\nabla\cdot\frac{h^3}{3\eta}\nabla\left[\frac{dg(h)}{dh}-\gamma\nabla^2 h\right]-\alpha\left[\frac{dg(h)}{dh}-\gamma\nabla^2 h-\mu(p)\right]. \tag{2}$$

The first part of Eq. (2), proportional to the inverse viscosity η^{-1} of the liquid film, describes a creeping motion of a thin-film flow on the substrate. Note that a relaxation term proportional to α has been added. This term alone guarantees that a homogeneous liquid film will relax to its equilibrium value by evaporation or condensation. For $h=h_\infty(p)$, this term vanishes. $\mu(p)$ is the chemical potential of the vapor.

In the (almost) dry area, the contributions of both terms to the total flow and evaporation of material can be basically neglected, because of the small value of h_-, typically less than one monolayer of adsorbed fluid. Inside the wet area, we can to lowest order linearize $h=h_\infty[1+u(x,y)]$, where u is now a small deviation from the asymptotic equilibrium value $h_\infty(p)$ in the liquid. Since $\nabla h_\infty(p)\equiv 0$, the only surviving terms are linear in u and its spatial derivatives ∇u and Δu. Therefore, inside the wet area, the evolution equation for the variable part u of the height variable h becomes

$$\frac{\partial u}{\partial t}=D_{\mathrm{eff}}\Delta u-\lambda_{\mathrm{eff}}u. \tag{3}$$

Here we have dropped the terms $\sim\gamma\Delta^2 u$ since the effective diffusion constant $D_{\mathrm{eff}}=(h_0^3/3\eta)\{d^2g/dh^2\}+\alpha\gamma$ is positive and dominates the long-wavelength behavior over the fourth-order term. The relaxation coefficient is $\lambda_{\mathrm{eff}}=\alpha\{d^2g/dh^2\}$. Derivatives are taken around the equilibrium value $h=h_0$. Note that Eq. (3) is precisely the equation of motion studied in [13], leading to seaweed patterns.

Of course, this approximation holds only inside the wet region, not directly at the dry-wet front. This interface region gives rise to a profile $h(x)$ similar to a tanh function. The rising of the tanh profile from the dry to the wet part occurs over a distance short compared to the typical patterns being observed in the dewetting process. In the so-called sharp-interface limit, we can replace this profile by a sharp interface between the dry and the wet part, but must add the corresponding boundary conditions to the equation of motion (3) for the wet side. Obviously, the boundary conditions consist of a conservation law that guarantees that a displacement of the dry-wet front must locally conserve the fluid. Under dewetting conditions, this leads to a swelling of fluid $u>0$ at the interface. The second condition clearly comes from the surface tension γ, which tends to keep the dry-wet front straight. This is just the usual Gibbs-Thomson condition for an interface, with the capillary length being approximately $d_0\approx\gamma/[\{d^2g(h)/dh^2\}\ell]$, where ℓ is the thickness of the dry-wet interface or front, and the dimensionless driving force is $\Delta=(h_0-h_\infty)/h_0$. In summary, we have for this viscous fluid-flow problem of surface dewetting exactly the same equations as for the diffusional growth of an isotropic solid.

III. HYDRODYNAMICS OF TWO-FLUID SYSTEMS

Incompressible hydrodynamic flows with a free interface as considered here are described by the incompressible Navier-Stokes equations

$$\frac{\partial \vec{u}}{\partial t} + (\vec{u}\cdot\nabla)\vec{u} = \frac{1}{\rho}(-\nabla p + \eta\Delta\vec{u} + \vec{f}_s), \tag{4}$$

$$\nabla\cdot\vec{u} = \mathbf{0}. \tag{5}$$

In these equations, $\vec{u}$ is the velocity vector and p is the pressure. The density ρ and the kinematic viscosity $\nu=\eta/\rho$ are constant inside each of the two fluids, but may vary discontinuously across the interface. The force $\vec{f}_s$ in principle can be an arbitrary local force field defined everywhere in space just like, for example, a gravitational force. Here we assume that it is a force localized at the interface between the fluid on the substrate and the gas. Any bulk force, which is the gradient of some fixed potential, will be immediately compensated by a change in the pressure and therefore gives no contribution to the equation of motion Eq. (4).

The question now is how can this interface be handled conveniently by numerical methods? We follow here concepts given in Refs. [14–16], together with some ingredients of our own experience in phase transformations [17]. We use here what is known in fluid dynamics as the *volume-of-fluid* approach [15,16,18–20], which in the theory of phase transitions corresponds to the *phase-field model* for two-phase systems and generalizations [21–23]. A consistent phase-field model with hydrodynamic flow was recently formulated [24]. This method smears out the sharp interface over some nonzero but finite thickness d_s, so that the material parameters do not jump discontinuously but vary continuously across that interface. Note that the thickness of this interface d_s between two phases in reality corresponds to a few atomic units. For computational purposes, it should therefore be small compared to all macroscopic lengths occurring in the model, since the Navier-Stokes equations correctly describe only macroscopic properties of hydrodynamic systems. We will return to this point in the discussion of the results.

In comparison with sharp-interface methods, one loses a factor approximately between 10 and 100 in computational efficiency, but the advantage of much simpler programming of multiphase problems seems to be worth the expenditure. Similar arguments hold for the alternative lattice-Boltzmann methods [25,26] or a recent molecular-dynamics study, where hole formation and the initial stage of dewetting has been simulated [27]. Both methods reconstruct the macroscopic equations from the microscopic dynamics of particle collisions. The computational efforts of these smeared-interface methods seem to be comparable. However, we prefer here the somewhat more direct and intuitive access by the phase-field approach.

The basic idea of the phase-field method is that a phase field ϕ varies across the liquid-gas interface continuously from $\phi=-1$ for the liquid to $\phi=1$ for the gas (the association of numbers to the phases is of course arbitrary; zero and one would also be possible). This variation takes place over the interface thickness d_s. The normal vector $\vec{n}$ to the interface is defined as

$$\vec{n} = \nabla\phi/|\nabla\phi|, \tag{6}$$

which can directly be used for numerical approximations when all fields are defined in discretized form on a regular lattice. Since the normal vector to the interface is only needed at the interface ($\vec{x}=\vec{x}_s$), we typically encounter a combination of normal vector and δ function, which can be described simply by

$$\vec{n}\,\delta(\vec{x}-\vec{x}_s) = \tfrac{1}{2}\nabla\phi. \tag{7}$$

With this definition, a surface force $\vec{f}_{s0}$ only due to the local curvature K of the interface and the surface tension γ is given by

$$\vec{f}_{s0} = \gamma K\vec{n}\,\delta(\vec{x}-\vec{x}_s). \tag{8}$$

This allows us to vary the surface tension γ independent of the phase-field parameters as compared with [24]. The practical evaluation of the curvature K is done via the definition that the curvature of a line (in two dimensions) is equal to the divergence of the field of normal vectors along that line. This can be generalized to a two-dimensional field of normal vectors as $K=\nabla\cdot\vec{n}$. The curvature is then evaluated everywhere in the $\{x,z\}$ plane by straightforward discretization. Finally, a smoothing operation is performed on the curvature field inside the interface region. This is done similarly to a diffusion time step so that the curvature field is almost constant in normal direction across the interface.

The phase field now couples to the Navier-Stokes equation (4) via the surface force (8),

$$\vec{f}_s = \vec{f}_{s0}, \tag{9}$$

and the Navier-Stokes equation couples back to an equation of motion for the phase field via an advection equation,

$$\frac{\partial\phi}{\partial t} = -\vec{u}\cdot\nabla\phi + F\{\phi\}. \tag{10}$$

A nonlinear operator $F\{\phi\}$ has been added here for numerical reasons in order to locally maintain a well-defined S-shaped profile of ϕ in normal direction across the interface, as will be made explicit below.

In principle, Eqs. (4)–(10) form a closed system of equations in space and time (with appropriate boundary and initial conditions, and assuming for the moment all materials parameters to be homogeneous and constant), apart from the evaluation of the pressure gradient ∇p in Eq. (4). We have used a simple marker and cell method (MAC) scheme for the moment, but plan to implement more complex schemes [16,20] in the near future to solve the Poisson equation, which one obtains for the pressure after applying a further divergence operator onto Eq. (4). We have also kept the densities in the liquid and in the ''gas'' equal for the moment, as

well as the kinematic viscosities. This may sound a bit unphysical at first, but it does not change substantially the basic physical problem of dewetting hydrodynamics, as we will discuss in the final section. The reason for this present simplification is just to facilitate computation (see, for example, [16]). Therefore, we will maintain the notion ''gas'' and ''liquid'' to discriminate between the phases, although their materials parameters for the moment are just equal.

The numerical implementation closely followed earlier experiences [16,20,28], with our simpler use of a MAC scheme and forward integration instead of multigrid-pressure evaluation and implicit [alternating-direction implicit method (ADI)] schemes, which we plan to incorporate in the future. As tests we have reproduced features described in [16]; furthermore, we have confirmed the dynamical spectrum of capillary surface waves within a few percent.

To close this section, we briefly describe the numerical method to keep a well-defined S-shaped interface profile in the ϕ variable by the operator $F\{\phi\}$ in Eq. (10). Based on previous experience with phase-field simulations, we define this nonlinear operator as

$$F\{\phi\}=\frac{1}{\tau}\{\xi^2\vec{n}\cdot\nabla(\vec{n}\cdot\nabla\phi)+V_0(\phi-\phi^3)\} \qquad (11)$$

with parameters $\xi=2,\tau=0.4,V_0=1$ (the precise values are not critical). Here ξ^2 multiplies a second-order derivative in normal direction across the interface, which has a tendency to smooth out the phase field, while the term with V_0 tries to keep ϕ as a step function $\phi=\pm1$. Note that in contrast to the usual phase-field models [17,21,24], we decompose the spatial variations of the phase field ϕ near the interface ($\phi\approx0$) into a part parallel to the interface and a part normal to the interface. The two Nabla operators in Eq. (11) only work in the direction normal to the interface. Dropping here the tangential terms in the spatial variations, we have a model with vanishing surface tension. This holds in the physically interesting limit, where the radius of interface curvature is larger than the interface thickness. We are therefore free to choose the interface free energy. In addition, the model may be used as a basis to study membranes, which have interface stiffness rather than interface tension.

In the stationary case (with $\vec{u}=0$), Eq. (11) together with Eq. (10) give a profile $\phi\approx\tanh(x_n/d_s)$ in normal direction across the interface, with well-defined interface thickness $d_s\approx\xi/\sqrt{V_0}$. In principle, this operator does not exactly conserve the quantity ϕ, so one should have once more a Laplacian operating over the whole right-hand side of Eq. (11). Since this would increase computing time, we used a simple modification to keep this effect small: In the space- and time-discretized version, we set this operator $F\{\phi\}$ exactly equal to zero during one time step if its absolute value throughout the computational lattice does not exceed a critical threshold of $\delta F_0=2$. Again, this numerical value is not critical. A circular droplet of radius $R\geqslant2.5$, for example, will not shrink to zero due to a remaining effective surface tension introduced by the discretization of Eq. (11). In total, we found all tests performed to be in sufficient agreement with the results given by Lafaurie *et al.* [16].

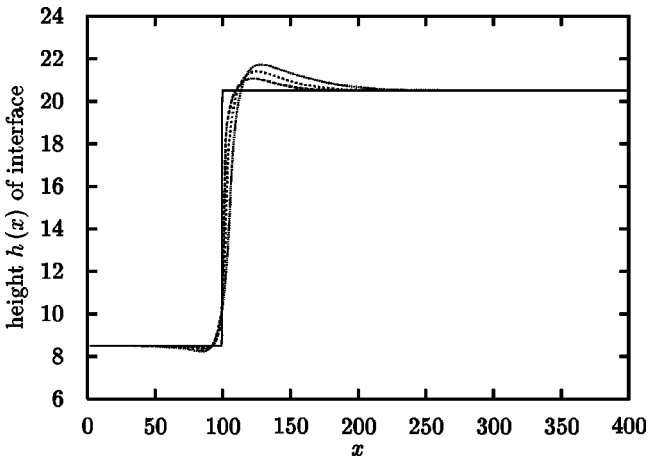

FIG. 1. Dewetting process in $1+1$ dimensions. The original front separating the dry and wet parts of the substrate was given as a step function, at lattice position 100. During the dewetting process, the front moves towards the wet part at the right. The units given here are lattice units, one lattice unit corresponding to one-half ''arbitrary unit'' ($dx=0.5$, $\nu=12$).

IV. HYDRODYNAMIC MODEL FOR WETTING

In this section, we now describe the specific modifications of the general hydrodynamic model introduced above in order to treat the wetting-dewetting process.

In equilibrium thermodynamics, partial wetting of a substrate means the possibility of a thin wet layer of finite thickness to exist on the substrate in coexistence with a dry part of the substrate and a gas phase above the liquid film. Since we want to model the front between the dry and the wet part by a tanh-like profile, we will describe the dry part by a height $h(x)$ of the wetting layer being almost zero, while for the wet part we assume a height of nonzero but finite thickness. Above that tanh-like profile, we have a pure vapor phase. Note that both the wet and the dry part of the substrate are covered with fluid, the difference being that the fluid layer on the ''dry'' part is much thinner (maybe even less than one atomic unit practically) than the wet part.

To be explicit, we show in Fig. 1 such a profile where the horizontal axis x is the position on the substrate while the vertical axis represents the height $h(x)$ or the direction away from the substrate in the normal direction. The units here are given in lattice units of the computational grid (400×30), which corresponds with a lattice constant of $dx=0.5$ ''physical'' units to 200×15 ''physical'' units of distance.

The initial profile is given as a step function jumping with increasing x at $x=100$ from $z=8.5$ to $z=20.5$, all values given in lattice units ($dx=0.5$). Note that the equilibrium height (to be defined below) of the wet part would correspond to 22.5 lattice units (corresponding to 11.25 ''physical'' units) so that the structure initially is in a nonequilibrium condition. Below and to the right of the step function of Fig. 1 is the ''liquid'' with $\phi=-1$; above and to the left is the ''gas'' phase with $\phi=+1$.

The equilibrium positions of the gas-liquid interface in the wet and the dry regions of the substrate are defined by an external double well potential $g(h(x))$ acting on the interface. It summarizes the Van der Waals and polarization forces due to the substrate and is explicitly described in [2,4,7,29]. However, for the study of scaling properties (which do not depend in detail on specific material properties) it is only necessary to identify the potential near its equilibrium positions. The equilibrium positions h_- and $h_\infty(p)$ result from a double-tangent construction to $g(h)$. To facilitate the location of these minima, we replaced this potential by a potential symmetrical in the two minima and sitting on the same energy level:

$$U_w = U_0 \sin(kz + kz_0). \tag{12}$$

It varies in direction normal to the substrate and is constant parallel to the substrate. This potential U_w corresponds to the potential $g(h(x,y))$ in Eq. (1), where the z coordinate in Eq. (12) corresponds to $h(x)$ in $g(h)$. (In our present work we only keep one spatial coordinate x at the moment.) Note that adding a constant gradient in Eq. (2) as $g(h) \rightarrow g(h) + ch$ with arbitrary c only changes the definition of the chemical potential $\mu(p) \rightarrow \mu(p) + c$ of the gas and therefore corresponds to a trivial change.

In principle, this potential should have only two minima, one within one atomic layer close to the substrate and one a distance of some 10^3 nanometers above the substrate. The one minimum corresponding to the gas phase very close to the substrate would be much narrower than the other one corresponding to the wet layer. For reasons of testing the numerical procedure, we took here a potential with fully symmetrical minima near $z = \{4.25, 11.25\}$ while the other oscillations of that sine potential were irrelevant within our numerical investigations.

This potential produces a force

$$\vec{f}_{s1} = \delta(\vec{x} - \vec{x}_s)\vec{n} \cdot [\vec{n} \cdot \nabla U_w(z)] \tag{13}$$

onto the interface between the liquid and the gas phase. The force is proportional to the gradient of the potential but acts in normal direction of the liquid-gas interface only, otherwise it would produce a constant tangential flow in interface regions with normal direction parallel to the substrate (Marangoni effect). In equilibrium, this force must compensate for the forces f_{s0} in Eq. (8) originating from interface curvature, which also act in normal direction to the interface.

The total force acting on the interface is then the sum of the curvature force Eq. (8) and the force originating from the external potential Eq. (13):

$$\vec{f}_s = \vec{f}_{s0} + \vec{f}_{s1}. \tag{14}$$

Some basic parameters were set as follows. The lattice consisted of typically 30 units in direction normal to the substrate and up to 1200 in a direction along the surface of the substrate.

The geometry was for the moment only two-dimensional. The lattice constant was set in physical units as $dx = 0.5$ or smaller and the time step for forward integration was chosen appropriately to guarantee the numerical stability of the differential equations involved. The surface tension was $\gamma = 3.18$ and the wall potential near the two minima was taken as $U_w = \sin(kz + kz_0)$ with $k = 2\pi/7$, $z_0 = 1$ and with minima relevant for the ''dry'' part and the ''wet'' part at $z = 4.25$, 11.25. This corresponds to a total thickness of the wet layer in coexistence with a dry surface part of $\delta h = 7$ in our physical units. Note that assigning specific values to the units of dx and dt fixes all length scales, the time scales, and velocities. In these units, the kinematic viscosity was set to values between $\nu = 0.5$ and 16; the density was set to $\rho = 1$.

The boundary conditions for the fluid were sticking conditions or velocity zero on both the bottom and on the sides of the grid. On the top of the grid we applied a fixed pressure condition (bearing in mind the incompressibility of the fluid), thereby granting a free-flow condition at the top.

The complete system of equations then are Eqs. (4)–(8) and Eqs. (10)–(14). We have confirmed numerically that the forces give a stationary nonmoving S-shaped front profile in the $\{x,z\}$ plane under equilibrium conditions as desired.

V. RESULTS AND DISCUSSION

An experiment on the dewetting transition ideally would start from an equilibrium condition with a dry and a wet part of the surface in coexistence. The heights of the liquid layer on the dry part would be practically zero, and of some finite value (of order of microns, for example) on the wet part. Nonequilibrium is then achieved by suddenly lowering the gas pressure above the substrate. The dry part of the substrate would not react significantly, while the wet part would evaporate to a new equilibrium at a somewhat lower height of the liquid layer.

This is the starting condition for our simulation: We keep the height of the dry part positioned in the minimum of the potential Eq. (12) close to the origin while the height of the wet part is shifted out of the minimum to a slightly smaller value.

In this situation, the dry part is energetically favorable so that the front between the dry and the wet part starts moving towards the wet part at the right in Fig. 1. Because of conservation of fluid on both sides of the liquid-gas interface, such a displacement of the wet-dry front leads to a redistribution of material thereby creating a pronounced bump. In the full three-dimensional scenario, this redistribution ultimately leads to the patterns observed in the dewetting experiments. Clearly in our still two-dimensional scenario, this pattern formation cannot be fully described, yet already basic predictions about the low viscosity behavior can be made, as will be seen below.

There are several physical parameters in the model including the density and the viscosity of the fluid, as well as a number of numerical parameters such as the constant V_0 in Eq. (11), which controls the shape of the smeared interface d_s between the liquid and the gas. The interface thickness d_s should be small compared to all physically relevant length scales, in order to obtain physically meaningful results. Clearly, this condition is not yet very well satisfied by our

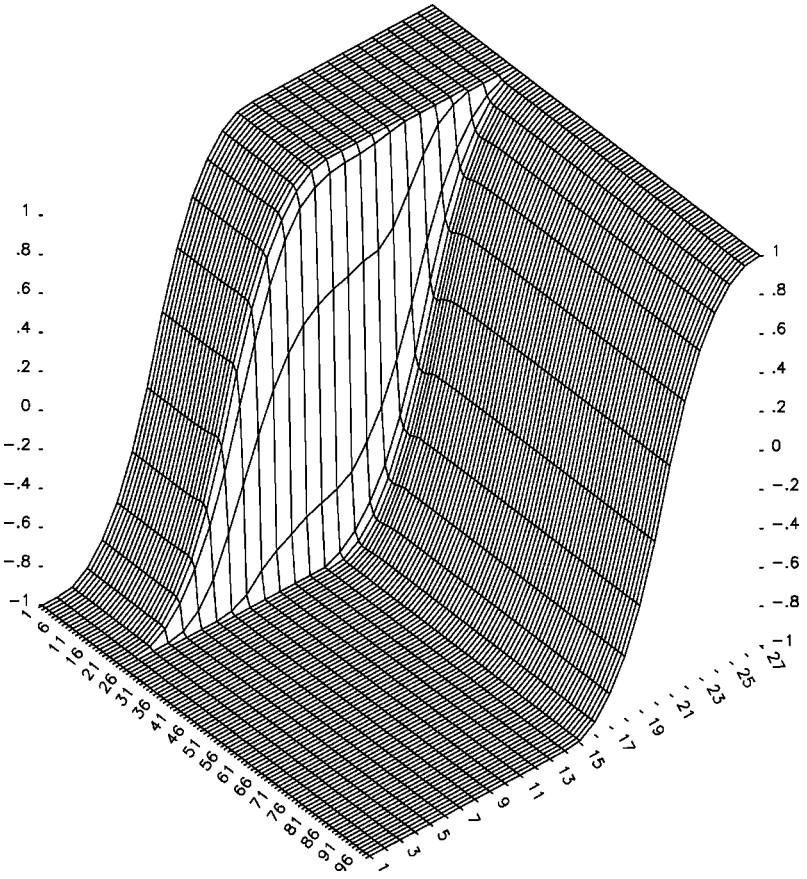

FIG. 2. Phase-field profile corresponding to Fig. 1. One sees the quick rising of the phase field from -1 to 1 in the dry region, and the latter rising at lattice units around 20 in the wet region to the right. (The lower left axis corresponds to the substrate or the horizontal axis of Fig. 1, the numbering $1,\ldots,96$ corresponding to every fourth lattice point. The numbering on the lower right axis corresponds to the numbering on the z axis of Fig. 1.)

presently rather small lattice. We have therefore made a number of numerical tests to check upon the validity of the results.

First we have checked circular bubbles moving in a flow field of constant velocity. The bubbles maintained their size within a few percent traveling over about 100 times their diameter. Bubbles would not shrink unless their initial radius was smaller than $R \leqslant 2$ (corresponding to four lattice units). We also noticed the occurrence of ''flotsam'' as mentioned in [16]. Furthermore, we have studied the temporal evolution of an interface separating the two fluids, with an initially sinusoidal capillary wave imposed onto the interface with wave number q. At sufficiently low viscosities, the amplitude of that deformed interface should make periodic oscillations with a frequency $\omega = \sqrt{\gamma/\rho} q^{3/2}$. As soon as the wavelength was bigger than about four times the thickness of the interface d_s, the agreement was within a few percent. This should actually be a rather sensitive test of the correctness of the code in general, as well as of the specific way of handling the free interface.

Also, we have checked the convergence of flat interfaces to the potential minima of Eq. (12). For this purpose, the local conservation laws for the two fluids had to be modified since otherwise a flat interface cannot move. We have introduced ''holes'' at both lateral ends of a flat interface parallel to the substrate, by switching off the coupling between fluid and phase field. Fluid then could flow from below the interface to above the interface and the interface would relax its position to either of the minima of U_w, while the total amount of fluid still was conserved. Finally, we have studied the possibility to generalize this model to incorporate phase transitions within the fluid phases together with the flow. For this purpose, the drift term $\vec{u} \cdot \nabla \phi$ in Eq. (10) was modified into $\vec{u}_{\rm eff} \cdot \nabla \phi$ with $\vec{u}_{\rm eff} = \vec{u} - \delta\vec{u}$, where $\delta\vec{u}$ was given externally representing some nonequilibrium driving force times a mobility for the advancement of a reaction front such as evaporation or condensation. All these tests gave stable and numerically reasonable results.

The full wetting-dewetting problem in $1+1$ dimensions was then investigated and compared with a model of Cahn-Hilliard-type. The latter model was defined as Eq. (2) with $\alpha = 0$ and the potential $g(h)$ taken as Eq. (12). This gives explicitly

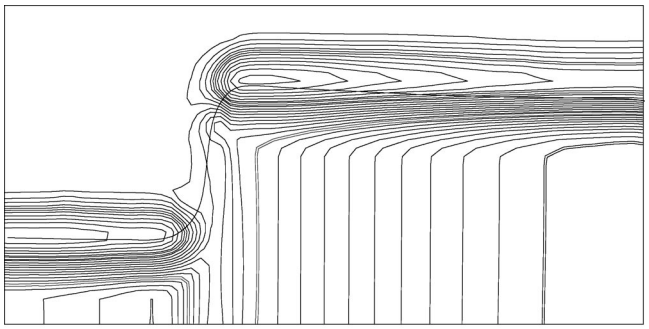

FIG. 3. Isobars corresponding to Fig. 1.

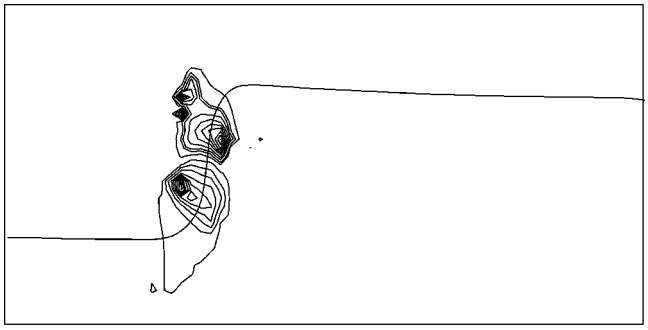

FIG. 4. Contours of constant curvature of the S-shaped front between the dry and the wet part corresponding to Fig. 1.

$$\frac{\partial h}{\partial t} = \nabla \cdot \frac{h^3}{3\eta} \nabla [k \cos(kh + kh_0) - \gamma \nabla^2 h] \tag{15}$$

with $k = 2\pi/7$ and $h_0 = 1$.

Note that all parameters in this model also occur in the full hydrodynamic wetting model described above. The results of direct simulations of the hydrodynamic model Eqs. (4)–(8) and Eqs. (10)–(14) are then given in Figs. 1–8.

In Fig. 1, we show the initial stages of the dewetting process, where the originally step-function shaped front develops a bump (in higher dimensions corresponding to a rim) and moves to the right towards the fluid layer. The boundary condition at the far right does not allow liquid to flow out of or into the system.

The pressure distribution is shown in Fig. 3. The most pronounced effect here again is due to the nonzero width of the horizontal parts of the interface between liquid and gas. The potential Eq. (12) tries to compress the smeared interface, which leads to localized pressure gradients. This effect should be less pronounced when the physically interesting length scales of the problem would be much larger than the computational length scales such as lattice constants and interface thickness d_s. The next plot of this series (Fig. 4) shows the two-dimensional curvature of the smeared interface. It is again a two-dimensional field due to the nonzero thickness of the liquid-gas interface. It is obviously located in the regions where the profile in Fig. 1 changes from the lower position on the left to the upper position on the right.

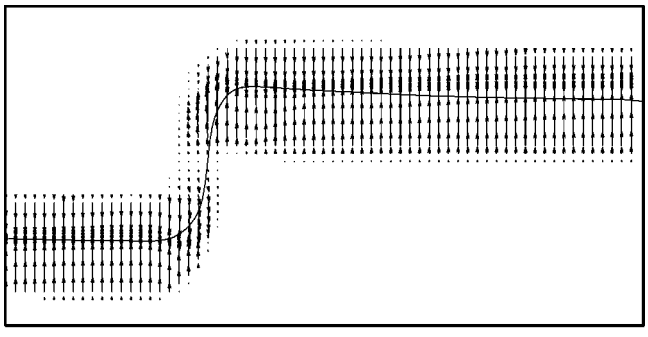

FIG. 5. Force field from Eq. (13) in the interface region corresponding to Fig. 1.

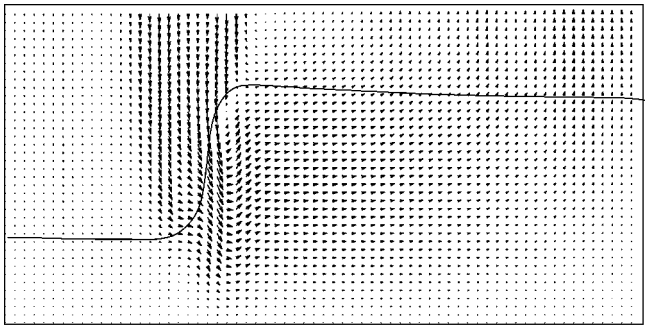

FIG. 6. Flow pattern corresponding to Fig. 1.

(Again one should note that the scales are distorted, as the full 400×30 grid points of the lattice are scaled within the frame displayed here.)

Figure 5 shows the force field resulting from Eq. (13). The rectangular area corresponds to the whole lattice now, 400 lattice units wide and 30 lattice units high. Note that the scales in the vertical and horizontal directions are not equal. One sees clearly the relatively wide area (in vertical direction) over which the force field is nonzero. This corresponds to the interface area of Fig. 2, where the phase ϕ differs from ± 1.

In Fig. 6, the corresponding flow pattern is indicated. The flow is most pronounced in the region directly behind the interface (where the height rises from about 8.5 lattice units to about 22 lattice units in Fig. 1), which leads to the formation of the bump by displacing ''liquid'' towards the right and upward.

Possibly the most interesting results are shown in Figs. 7–9. In Fig. 7, three curves of the displaced interface profile

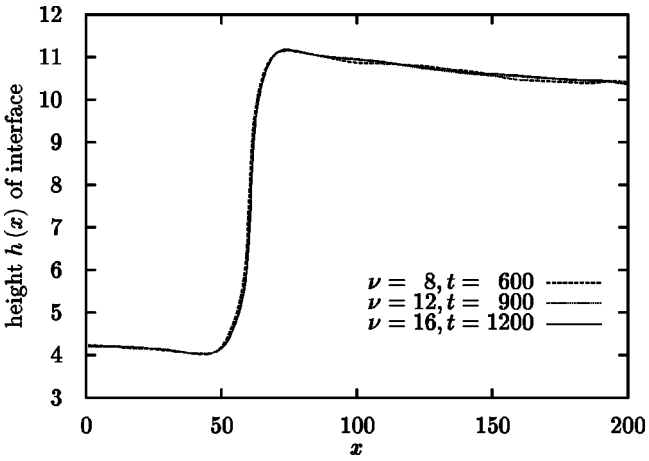

FIG. 7. Dewetting process in 1+1 dimensions, as in Fig. 1. Comparison of three different viscosities $\nu = 8,12,16$ at times $t = 600$, 900, 1200, respectively. The results should fall on one curve if observation times are chosen to be proportional to ν. Apart from the small wiggles in the tail of the front that result from the high lattice constant of $dz = 0.5$, this property is fulfilled quite well. Taking the height of the film $h = 7$ as a characteristic length scale, the effective Reynolds numbers reached here are Re = 0.11, 0.05, 0.03. All units were given in physical units with a corresponding lattice spacing of $dx = dz = 0.5$.

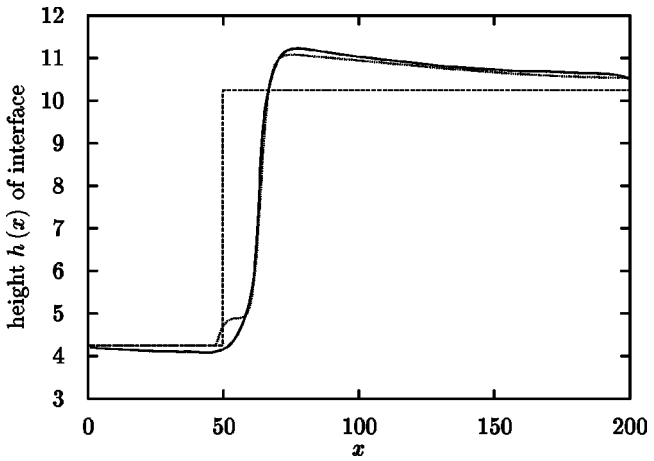

FIG. 8. Dewetting process in $1+1$ dimensions (full line), as in Fig. 1, but now at a later time $t=1000$ (physical units). In comparison, we show the result from the diffusion model Eq. (15) (dotted line). Again the original front between the dry and the wet part of the substrate was given as a step function (dashed line). During the dewetting process, the front moves towards the wet part, forming a distinct bump on the wet side to the right of the moving front. The agreement is quite satisfactory, since there were no adjustable parameters. All units were given in physical units, while the underlying lattice constants were $dx=0.5$ and $dz=0.125$. The kinematic viscosity was set to $\nu=12$.

are shown for three different viscosities $\nu=\{8,12,16\}$ at observation times $t=\{600,900,1200\}$, respectively. All three results fall on one curve, which is to be expected since the observation times are chosen to be proportional to ν. For smaller viscosities $\nu\lesssim 1$ the tail of the front tends to form pronounced wiggles whose asymptotic time behavior is not cleared completely for the time being (see Fig. 9). Small viscosities are somewhat problematic in this geometry since the physical length scales of the resulting vortices are no longer large compared to the present grid size and the interface thickness d_s.

In Fig. 8 we compare the results of the diffusional Cahn-Hilliard model for wetting-dewetting, Eq. (15). The parameters for the two models were identical as far as the correspondence given by Eq. (15) holds. The agreement reached hereby in Fig. 8 is within about 10% for all relevant observables, which we take as quite satisfactory confirmation of the reciprocity of these two models for sufficiently large viscosities.

Figure 9 shows the same scenario as Fig. 7 for a somewhat smaller viscosity. It is clearly visible that the hydrodynamic aspect of the dewetting process is much more pronounced than before. The interface ''overshoots'' towards the equilibrium height and gives rise to spatial oscillations at

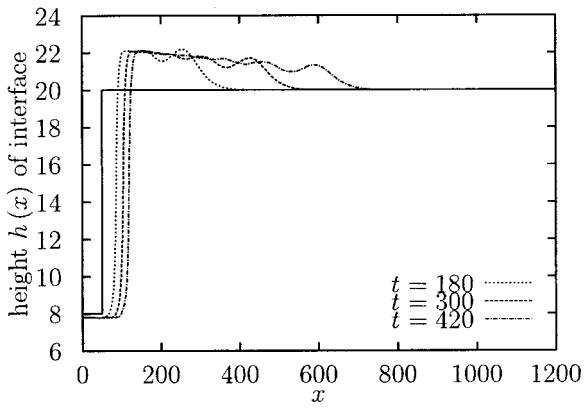

FIG. 9. Dewetting process in $1+1$ dimension as in Fig. 7, but with viscosity $\nu=0.5$ at times $t=180$, 300, 420, respectively. The physical length scales have been increased in order to minimize effects of the interface width. All units are given in physical units. Effective Reynolds numbers are of order 3.

least as a transient phenomenon. Nevertheless, the average shape of the slope is still determined by the limited amount of fluid that is transported to the right due to viscous friction.

In summary, we have demonstrated the feasibility of this kind of dewetting problem with a new phase-field approach. We have shown that the $(1+1)$-dimensional hydrodynamic model for dewetting is in reasonable quantitative agreement with an effective diffusion model for dewetting dynamics at least in the range of Reynolds numbers of order unity and below. For higher Reynolds numbers, the appearance of surface wiggles modifies the shape of the interface and creates a pronounced deviation from the viscous-creeping limit. These wiggles are to be expected in the fully three-dimensional case and could change the pattern-formation process significantly.

We are currently extending these simulations to the fully three-dimensional situation, employing more efficient integrators as ADI and multigrid methods, which we partly had already used in previous phase-field model calculations. This should allow for a comparison of pattern formation behavior in the limit of low and high Reynolds numbers.

ACKNOWLEDGMENTS

We thank M. Mihelcic and K. Wingerath for providing us with an early version of their MAC code, which was used as a basis for this program. We thank Y. Saito and M. Alaga-Bogdanovic for discussions. We thank F. Gutheim and R. Spatschek for their support in testing and modifying the program code. This work was partly supported by grants from the DFG, and we appreciate support by the John von Neumann center for supercomputing at Forschungszentrum Jülich.

[1] G. Forgacs, R. Lipowsky, and T.M. Nieuwenhuizen, in *Phase Transitions and Critical Phenomena*, edited by C. Domb and J. Lebowitz (Academic Press, London, 1991), Vol. 14.

[2] P.G. de Gennes, Rev. Mod. Phys. **57**, 827 (1985).

[3] F. Brochard-Wyart and J. Daillant, Can. J. Phys. **68**, 1084 (1990); C. Redon, F. Brochard-Wyart, and F. Rondelez, Phys. Rev. Lett. **66**, 715 (1991).

[4] A. Sharma and A.T. Jameel, J. Colloid Interface Sci. **161**, 190

(1993); **164**, 416 (1994).
[5] Jacob Israelachvili, *Intermolecular and Surface Forces*, 2nd ed. (Academic Press, London, 1991).
[6] N. Samid-Merzel, S.G. Lipson, and D.S. Thannhauser, Physica A **257**, 413 (1998).
[7] N. Samid-Merzel, S.G. Lipson, and D.S. Thannhauser, Phys. Rev. E **57**, 2906 (1998).
[8] K. Jacobs, S. Herminghaus, and K.R. Mecke, Langmuir **14**, 965 (1998); S. Herminghaus, K. Jacobs, K. Mecke, J. Bischof, A. Fery, M. Ibn-Elhaj, and S. Schlagowski, Science **282**, 916 (1998).
[9] G. Reiter, Phys. Rev. Lett. **68**, 75 (1992); Langmuir **9**, 1344 (1993).
[10] T. Ihle and H. Müller-Krumbhaar, Phys. Rev. Lett. **70**, 3083 (1993); Phys. Rev. E **49**, 2972 (1993).
[11] J.W. Cahn and J.E. Hilliard, J. Chem. Phys. **31**, 688 (1959).
[12] E.A. Brener, H. Müller-Krumbhaar, D. Temkin, and T. Abel, Solid State Ionics **131**, 23 (2000).
[13] T. Ihle and H. Müller-Krumbhaar, J. Phys. I **6**, 949 (1996).
[14] E.G. Puckett, A.S. Almgren, J.B. Bell, D.L. Marcus, and W.J. Rider, J. Comput. Phys. **130**, 269 (1997).
[15] J.U. Brackbill, D.B. Kothe, and C. Zemach, J. Comput. Phys. **100**, 335 (1992).
[16] B. Lafaurie, C. Nardone, R. Scardovelli, and S. Zaleski, J. Comput. Phys. **113**, 134 (1994).
[17] A. Boesch, O. Shochet, and H. Müller-Krumbhaar, Z. Phys. B: Condens. Matter **97**, 367 (1995).
[18] N. Ashgriz and J.Y. Poo, J. Fluid Mech. **221**, 183 (1990).
[19] J. Qian and C.K. Law, J. Fluid Mech. **331**, 59 (1997).
[20] M. Rieber and A. Frohn, *Proceedings of the 7th International Symposium on Comput. Fluid Dynamics, Beijing, 1997* (International Academic, Beijing, 1997).
[21] A.A. Wheeler, B.T. Murray, and R.J. Schaefer, Physica D **66**, 243 (1993).
[22] A. Karma and W.J. Rappel, Phys. Rev. E **53**, 3017 (1996).
[23] T. Abel, E. Brener, and H. Müller-Krumbhaar, Phys. Rev. E **55**, 7789 (1997).
[24] D. Jacqmin, J. Comput. Phys. **155**, 96 (1999).
[25] D.H. Rothman and S. Zaleski, Rev. Mod. Phys. **66**, 1417 (1997).
[26] O. Theissen, G. Gompper, and D.M. Kroll, Europhys. Lett. **42**, 419 (1998).
[27] J. Koplik and J.R. Banavar, Phys. Rev. Lett. **84**, 4401 (1999).
[28] M. Mihelcic, K. Wingerath, and Ch. Pirron, J. Cryst. Growth **69**, 473 (1984); M. Mihelcic and K. Wingerath, *ibid.* **71**, 163 (1985).
[29] L.D. Landau and E.M. Lifschitz, *Statistical Physics* (Pergamon Press, Oxford, 1980).